Contents lists available at ScienceDirect

Electric Power Systems Research

journal homepage: www.elsevier.com

MPPT in PV systems under partial shading conditions using artificial vision

Aranzazu D. Martin[a,*], Jesus R. Vazquez[a], J.M. Cano[b]

[a] University of Huelva, Spain
[b] University of Seville, Spain

ARTICLE INFO

Keywords:
Artificial vision
Backstepping control
DC/DC converter
MPPT algorithm
Photovoltaic system

ABSTRACT

Maximum power point tracking (MPPT) algorithms should track and extract the maximum power from photovoltaic (PV) systems under any environmental conditions. Most of conventional MPPT methods are able to reach the maximum point when there is only one peak in the P–V characteristic curve but they fail when the solar cells are affected by partial shading conditions due to the fact that multiple peaks appear in the P–V curve. Thus, a local maximum may be reached instead of the global peak. In this work, a new method to accomplish the maximum power point (MPP) under partial shading conditions using artificial vision is presented. The artificial vision uses a webcam to identify in real time the shadow irradiance and provide the reference voltage that supplies the maximum power, regardless of the number of peaks that the P–V curve presents. Then, the reference voltage is used by a robust and non-linear control, the backstepping controller, to regulate the DC/DC converter input voltage and to guarantee the PV modules maximum energy extraction. Experimental tests carried out outdoor validate the proposed method, obtaining a MPP tracking efficiency that ranges from 98.1% to 99.6%.

1. Introduction

Photovoltaic systems have become widespread everywhere as a way to extract the maximum energy from solar cells. Thus, the performance enhancement of these systems is one of the main aims of the MPPT algorithms to achieve the MPP. The power generated by PV systems depends on the temperature and the incident irradiance. Under uniform irradiance, the PV modules characteristic curves present only one maximum [1]. Conventional MPPTs are able to reach this peak [2]. However, partial shading conditions can lead to obtain several maxima in the PV systems P–V curves and the former MPPT algorithms may fail to achieve the MPP.

The mismatch concern is one of the main causes of losses in the power extraction from PV systems. They are originated from the interconnection of solar cells with different properties or under different conditions [3]. Therefore, the solar cell under the worst condition, i.e. the one that supplies the lowest energy, determines the PV array global output power. There are various types of mismatch losses, such as short-circuit current or open-circuit voltage. The most common and damaging kind is the short-circuit current, caused by the solar module partial shading [4,5].

The partial shading conditions are originated by the shadows of adjacent buildings, trees, moving clouds or even fast changes in the irradiance. Under partial shading conditions, a PV module is exposed to different values of irradiance and the shaded cells absorb the energy supplied by the unshaded cells exposed to higher irradiance, leading to highly localized power dissipation and converting this power into heat. Thus, the power generated by the partially shaded modules is much lower than the energy generated by unshaded PV cells. This may be detrimental to the PV modules and the performance of the PV system is seriously deteriorated, being this effect widely studied [6–8]. Therefore, bypass diodes are usually connected across the solar modules [9], to prevent the shaded PV modules from consuming the power generated by the unshaded modules. Then, the current flows through an alternative path when there are shaded solar cells. As a consequence of using bypass diodes, the PV array I–V and P–V curves may present multiple power peaks under non-uniform irradiance, complicating the tracking of the MPP [10,11].

Conventional MPPT algorithms are ineffective because they are not able to distinguish the global maximum from the local maxima. Lately, different MPPT methods have been modified to improve the tracking of the MPP, such as the Perturb and Observe algorithm [12], the incremental conductance method [13], the neural network method and

* Corresponding author.
Email address: aranzazu.delgado@die.uhu.es (A.D. Martin)

https://doi.org/10.1016/j.epsr.2018.05.005
Received 8 July 2016; Received in revised form 9 April 2018; Accepted 4 May 2018
Available online xxx
0378-7796/

fuzzy logic controllers [14,15], or the differential evolution of particle swarm optimization [16]. Other methods are based on the modifications of the number and/or configuration of the bypass diodes [17], others on the measurement of the PV array open-circuit voltage, the short-circuit current or the irradiance [18], amongst others [19]. Besides, there is a method that uses a thermography camera [20].

In this work, a new method using artificial vision to track the maximum power in real time is proposed to detect the shadow irradiance and provide the reference voltage that supplies the MPP. Artificial vision is commonly used in many real-time applications such as tracking systems to detect vehicles or even people, surveillance, military missions, video communication or videogames [21–23]. In this case, this technique is used to identify the partially shaded solar cells in a robust and fast way, detecting the irradiance of the shadows, the changes of shape and the shaded area in real time.

All the MPPT methods mentioned above reach the global maximum power point. The artificial vision algorithm is proposed because it is simple to implement. It also uses a low-cost camera and a low-cost microcontroller whereas other methods employs DSPACE [14], more expensive than the dsPIC. The duration of the convergence to the MPP of the artificial vision is shorter than Refs. [12] and [16], which presents fluctuations before reaching the MPP. The proposed control only requires one voltage sensor and one current sensor whereas Ref. [17] needs more sensors and it obtains a lower efficiency. Besides, Ref. [20] uses a termography camera. This camera is about 200 times more expensive than the camera used in the artificial algorithm vision.

Finally, a robust non-linear backstepping controller proposed by the authors [24–26], is used to regulate the PV modules output voltage. It controls the duty cycle of the DC/DC converter to reach the MPP taking into consideration the voltage given by the artificial vision.

The method is implemented in Matlab-Simulink environment since this software is proved to work [27–31]. This environment is appropriate to simulate the photovoltaic system conditions and environmental conditions.

2. Photovoltaic system

The used system in this paper is presented in Fig. 1. It shows series-connected PV modules and they are supervised by a webcam. The PV modules output is connected to a DC/DC power converter whereas the converter output is connected to a load.

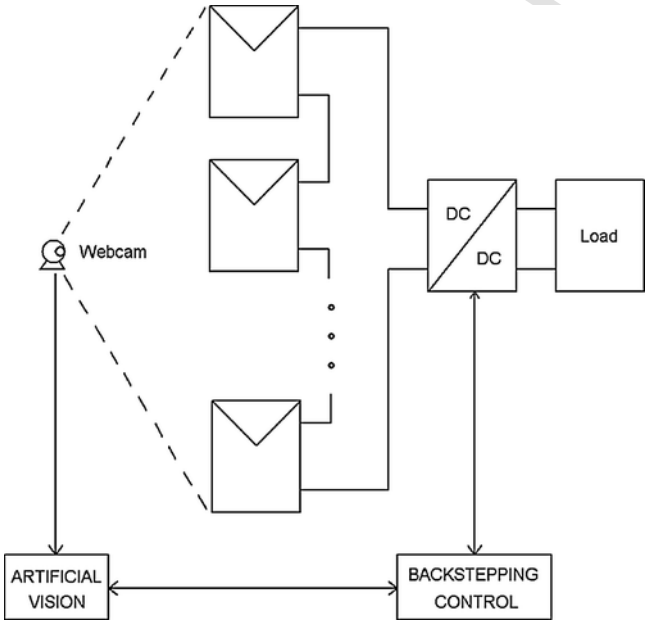

Fig. 1. Photovoltaic system with webcam to detect shadows.

The PV modules are series connected and the main problem of this configuration is a significant power drop when a solar cell or a group of cells are affected by the slightest shadow. Bypass diodes, which reduce the impact of mismatch losses from modules connected in series, are connected in anti-parallel with each solar module. Thus, the current flows through these diodes when the PV modules are shaded.

2.1. PV modules

In this work, commercial PV modules are used to validate the proposed method. The PV modules (one PV module consists of 36 solar cells connected in series) electrical features are presented under standard conditions, 25 °C and 1000 W/m^2, in Table 1. The maximum power that one PV module can supply is 20 W.

Fig. 2 presents the experimental I–V and P–V curves of a PV module under different values of uniform irradiance and temperature. The use of the bypass diodes implies P–V curves with multiple peaks when non-uniform conditions are presented, Fig. 3. In this work, three PV modules have been connected in series. Thus, the P–V curves may have a different number of peaks; it ranges from only one peak (when there are uniform conditions, Fig. 2) to three peaks (when each solar module is affected by different irradiance values). Fig. 3 shows the curves for various scenarios where the maximum power peak is located in different areas of the P–V curve, comparing the simulated model in Matlab-Simulink with real values to verify the results. Fig. 3(a) depicts a three-peak P–V curve where the MPP is located at about 15 V. Fig. 3(b) shows another three-peak P–V curve with the global maximum situated in approximately 36 V whereas Fig. 3(c) presents the global maximum in 56 V. Finally, Fig. 3(d) depicts a two-peak P–V curve because only one PV module is affected by a shadow and the MPP is located at 32 V.

2.2. DC/DC power converter

A DC/DC converter is used to control the PV modules output voltage. Thus, the maximum power must be tracked extracted. A built buck–boost converter is used [26], and it consists of power electronic components such as two capacitors, an inductor, a transistor and a diode, behaving as a non-linear load, connected as shown in Fig. 4. i_L is the inductor current, i_{PV} is the PV array output current, v_0 is the DC/DC converter output voltage, L is the inductor and it has a value of 780 μH, and C_1 and C are the capacitors, with a value of 1 mF.

The equations that model the buck–boost converter are presented in Eqs. (1) and (2). Eq. (1) presents the time derivative of the DC/DC converter input voltage and Eq. (2) is the time derivative of the inductor current.

$$\dot{v}_{PV} = \frac{i_{PV} - i_L D}{C_1} \tag{1}$$

$$\dot{i}_L = \frac{v_o}{\mathrm{L}} + \frac{v_{PV} - v_o}{\mathrm{L}} D \tag{2}$$

Table 1
Electrical parameters of PV modules.

Parameter	Values
Maximum power (P_{max})	20 W
Maximum voltage (V_{MPP})	17.5 V
Maximum current (I_{MPP})	1.15 A
Open-circuit voltage (V_{oc})	21.6 V
Short-circuit current (I_{sc})	3.31 A

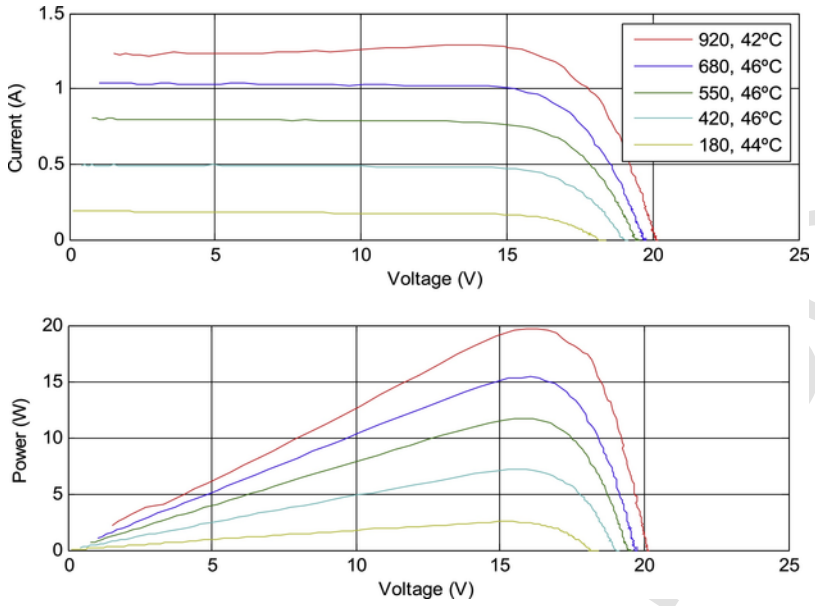

Fig. 2. I–V and P–V curves of a PV module.

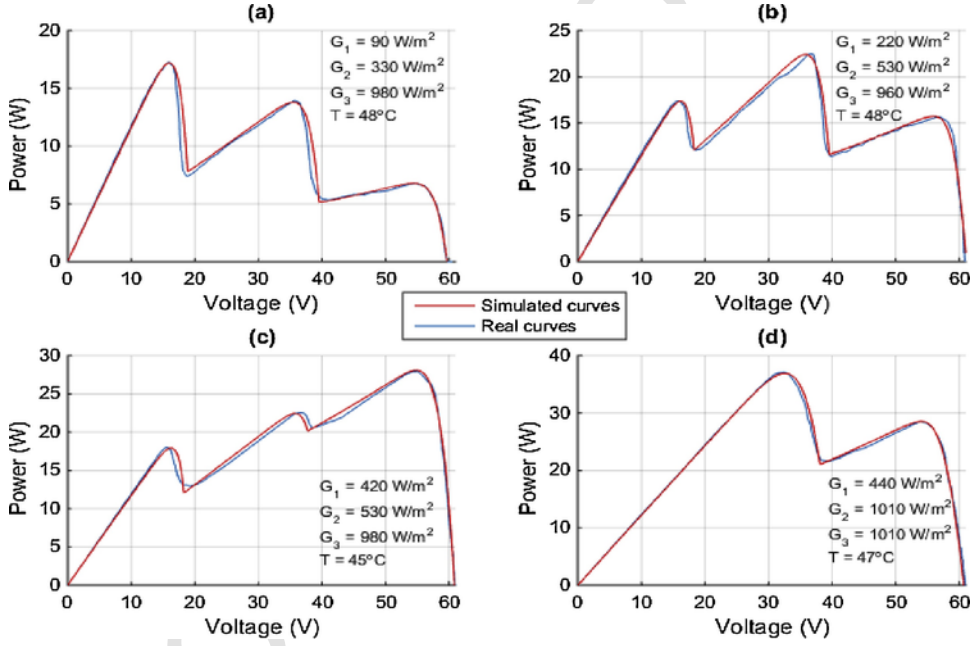

Fig. 3. P–V curves of the PV system under partial shading conditions.

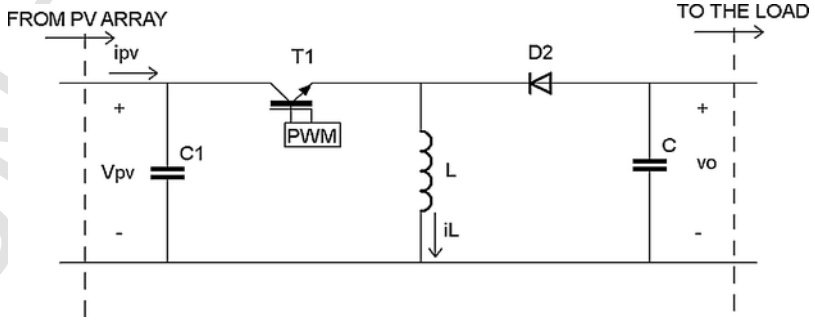

Fig. 4. Buck–boost converter.

A non-linear backstepping control, explained in Section 3, implemented in a low-cost microcontroller regulates the buck–boost converter input voltage, v_{PV}, modifying the DC/DC converter duty cycle, D, to achieve the voltage that provides the maximum power.

3. MPPT through artificial vision

In this paper, the MPPT algorithm employs an artificial vision algorithm and a backstepping controller. The artificial vision purpose is to identify the partial shading that affects the PV modules to provide the reference voltage that supplies the maximum power to the backstepping control. Therefore, the backstepping controller regulates the PV array output voltage using the reference voltage given by the artificial vision algorithm to reach the MPP under non-uniform irradiance.

3.1. Artificial vision

Webcams are commonly used in PV power plants as surveillance systems. Thus, this new method proposes to take advantage of this webcam to detect the shadows affecting the PV modules since any webcam or camera can be used for this proposal and it is not required special features.

To explain the algorithm it is required to define two new parameters, the shadow intensity and the shadow irradiance. The shadow intensity, I_{sPVj}, is obtained from the images received by the webcam and it is defined as the average value of the grey level of the area pixels contained in the blob area (region of adjacent pixels with similar properties), i.e. it is obtained dividing the result of the addition of every pixel intensity level by the number of pixels of the blob, as Eq. (3) expresses, where n is the number of pixels contained in the blob and j represents the number of PV modules.

$$I_{sPVj} = \frac{\sum_{i=1}^{n} grey\ level(i)}{blob\ area} \tag{3}$$

The shadow intensity values range from 0 to 100, where 0 is the no-shadow value (the shadow intensity for the unshaded PV modules is 0) and 100 is the maximum level of darkness, and they are related to the grey level. The shadow intensity is expressed as the grey percentage. The PV modules temperature is not required to calculate I_{sPVj}.

When I_{sPVj} is obtained, the shadow irradiance, G_{sPVj}, incident on the PV modules is calculated taking into consideration the shadow intensity according to Eq. (4), where j represents the number of PV modules.

$$G_{sPVj} = \hat{G}e^{-(0.0306 I_{sPVj})} \tag{4}$$

The shadow irradiance is an attenuation of the irradiance incident on the shaded solar modules, i.e. it measures the irradiance of the shadow. Eq. (4) is experimentally obtained using different shadows and values of irradiance, where $\hat{G}$ is the estimated irradiance. The PV modules measured temperature is considered to obtain the estimated irradiance. If there are unshaded PV modules, their shadow intensities are zero and their shadow irradiances are given by the estimated irradiance.

Fig. 5(a) presents the real value measurements (red points) of the shadow irradiance for different values of shadow intensity obtained using artificial vision. Moreover, this figure shows an adjustment curve (blue curve) for those points, obtaining Eq. (4). This expression is validated for different points with other shadow irradiances and shadow intensities and their models are depicted in Fig. 5(b).

The shadow detector output is the shadow irradiance for each PV module. Finally, the shadow irradiance should fulfil Eq. (5), where G_o is a variable that stores the estimated irradiance when there is no shadow. G_o will be only used if there are shadows. Under partial shading conditions, the estimated irradiance takes the last value of the estimated irradiance when there were no shadows. This value is saved in the variable G_o.

$$\begin{aligned} &If\ there\ is\ no\ shadow \\ &G_o = \hat{G}\ and\ G_{sPVj} = \hat{G} \\ &else \\ &\hat{G} = G_o\ and\ G_{sPVj} = \hat{G}e^{(-0.0306 I_{sPVj})} \end{aligned} \tag{5}$$

Then, the artificial vision MPPT (AVMPPT) algorithm proposed to identify the partial shading is presented in Fig. 6. The programming language is C and "opencv" and "cvblob" open source libraries are used. As shown the flow chart in Fig. 6(a), the first step is to select the images that may be affected by the shadows, i.e. each PV module, defining the region of interest (ROI). Then, the image is converted to Hue–Saturation–Value (HSV) color format [21]. This type of format is used because is much better handling lightning differences than the

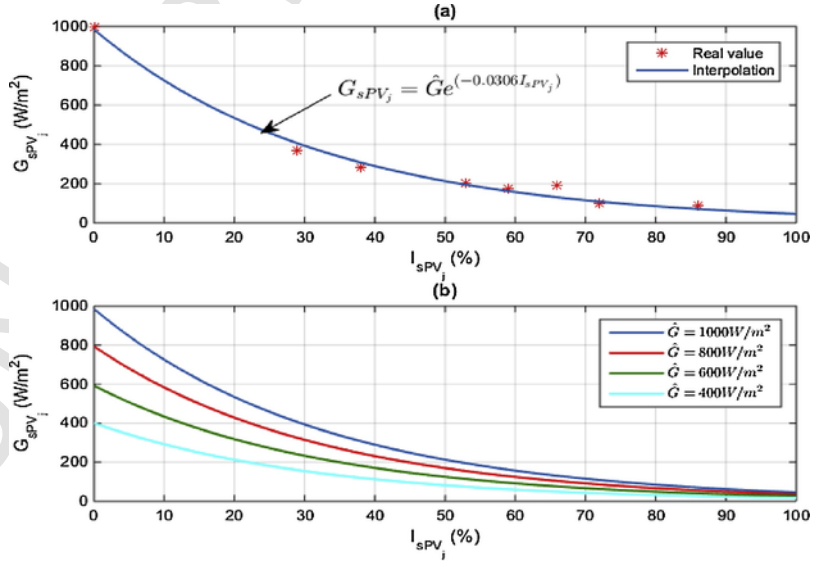

Fig. 5. Shadow irradiance. (For interpretation of the references to color in the text, the reader is referred to the web version of this article.)(a) Equation that models the shadow irradiance.(b) Shadow irradiance model under different values of estimated irradiance.

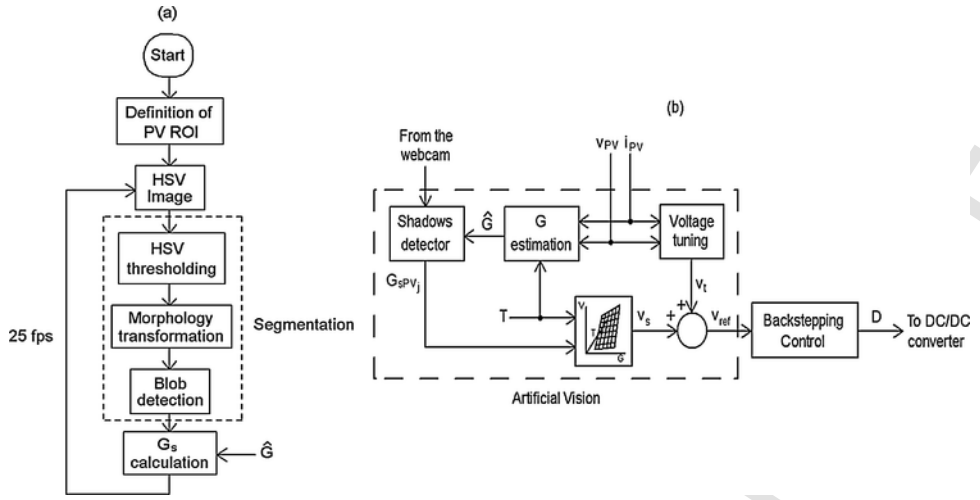

Fig. 6. Artificial vision algorithm.(a) Artificial vision algorithm flow chart.(b) Calculation of the shadow irradiance, GsPVj, and the reference voltage.

red, green and blue (RGB) values, obtaining a more robust color thresholding.

Afterward, the segmentation process starts and it is divided into three parts: the HSV thresholding, the morphology transformation and the blob detection. The first part is the image thresholding that modifies the HSV thresholds to select the color range that it is related to the shadows and to eliminate the information that it is not significant, obtaining a binary image. The second part, the morphological transformation, is the responsible for the filtering noise (removing isolated pixels) using an opening method, with a 2×2 matrix. The opening method consists of an erosion (it erodes away the boundaries of foreground objects and all the pixels near the limits are discarded depending on the size of the matrix) followed by dilation (it increases the region or size of foreground objects, filling up the remaining gaps) [22]. Then, the third part is the blob detection [23]. It identifies the blob area using an area filtering that allows for selecting the shadow minimum size to be taken into consideration.

Fig. 7 depicts the segmentation process running in the PV system. Fig. 7(a) shows the webcam capture when a PV module is partially shaded (ROI). Fig. 7(b) presents the shadow detection by means of the HSV thresholding. The shaded area is identified in white and the opening filter removes the isolated pixels. Finally, Fig. 7(c) shows the blob detection, delimiting the adjacent pixels with the same properties.

Next step in the flow chart, Fig. 6(a), is to calculate the intensity of the shadows with the help of the estimated irradiance, $\hat{G}$. Finally, the reference voltage that supplies the MPP, v_{ref}, is obtained taking into account the sensor measurements, T, v_{PV} and, i_{PV}.

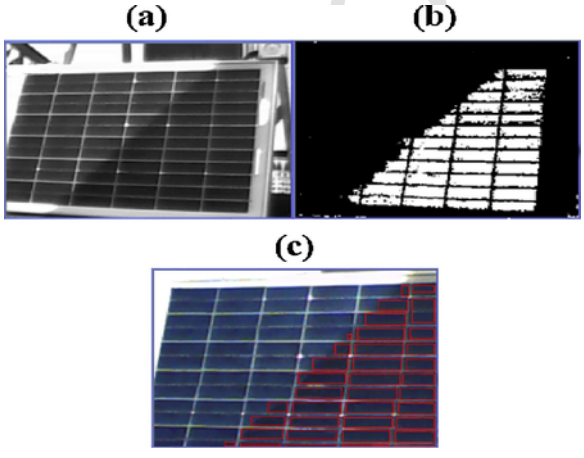

Fig. 7. Artificial vision algorithm.(a) Camera caption, ROI.(b) HSV thresholding.(c) Blob detection.

The last two steps of the flow chart are detailed in Fig. 6(b). An estimation of the irradiance can be accomplished from the measurement of the temperature and PV array output voltage and current. Hence, a regression plane is built to obtain the estimated irradiance. Using $\hat{G}$ and Eq. (4), the shadow irradiance of each PV module is calculated. Then, a theoretical voltage, v_s, that supplies the maximum power considering the temperature and the shadow irradiance is achieved with the help of a regression plane, [25,26], leading the seeking algorithm directly to the area where the MPP is located at the P–V curve. Thus, the local maxima originated by partial shading conditions are avoided. This theoretical voltage is adjusted to reach the real value of the MPP, obtaining the reference voltage required by the backstepping control. For that, a voltage tuning is considered to take the theoretical voltage to the optimum value. The tuning, [25], provides an incremental value of the voltage, v_t. Therefore, the addition of v_s and v_t supplies the reference voltage, v_{ref}. This reference voltage updating is fixed to 10 ms, such as the sensor measurements for the temperature and the PV modules output voltage and current.

3.2. Backstepping control

Backstepping controls are responsible for the achievement of control laws for the systems, in this case, for the buck–boost converter. These non-linear controllers use a recursive methodology to the model direct dynamics to guarantee the stability and robustness of the system by means of Lyapunov functions.

The main aim of this controller is to regulate the PV modules output voltage to enforce the PV modules operation at the maximum power, controlling the buck–boost converter duty cycle. For that, the reference voltage given by the artificial vision is used. To accomplish this, the backstepping method works as follows: a current inner control loop controls the inductor current, i_L; then, a voltage outer control loop is the responsible for controlling the buck–boost converter input voltage, v_{PV}, generating the inductor reference current, α_1, used by the inner loop to control the inductor current; and finally, in a recursive way, the DC/DC converter duty cycle is defined by the current inner loop to track the inductor reference current, [24–26]. The used Lyapunov functions are globally positive-definite and their negative time derivatives guarantee the solution is globally asymptotically stable.

Thus, taking into consideration the buck–boost equations, (1) and (2), the backstepping method is applied and the controller obtained is presented in Eq. (6) [24–26], where e_1 is the defined

voltage error to stabilize the buck–boost to the origin enforcing the buck–boost input voltage v_{PV} to track the PV array MPP reference voltage $v_{PV}{}^{r}$, $e_1 = v_{PV} - v_{PV}{}^{r}$. z_1 is the defined current error to make the inductor current i_L be equal to its reference current to achieve a zero-tracking error, $z_1 = i_L - \alpha_1$.

To guarantee stability, the constant k_1 must be positive to make the time derivative of the Lyapunov function be negative, $\dot{V}_1 = e_1\dot{e}_1 = -k_1 e_1$. In this case k_1 is 5. Therefore, k_2 must be also constant and positive to make the time derivative of the Lyapunov function be negative, ensuring stability, $\dot{V}_2 = e_1\dot{e}_1 + z_1\dot{z}_1 = -k_1{e_1}^2 - k_2{z_1}^2$. The value of k_2 is 75. The controller gain values have been achieved empirically.

$$\dot{D} = \frac{1}{\alpha_1}\left[-\frac{v_o}{\mathrm{L}}D - \frac{v_{PV} - v_o}{\mathrm{L}}D^2 - e_1\left(\mathrm{C}_1{k_1}^2 - \frac{D^2}{\mathrm{C}_1}\right) + z_1\left(k_1 - k_2\right)\mathrm{D} - \mathrm{C}_1\ddot{v}_{PV}{}^{r} + \dot{i}_{PV}\right] \tag{6}$$

Then, $0 < D < 1$ and $\alpha_1 \neq 0$ and its expression is presented in Eq. (7). The time integral of this equation controls the buck–boost converter input voltage to reach the MPP.

$$\alpha_1 = \left(\mathrm{C}_1 k_1 e_1 + i_{PV} - \mathrm{C}_1\dot{v}_{PV}{}^{r}\right)\frac{1}{D} \tag{7}$$

4. Experimental tests and results

Experimental tests have been carried out outdoor to validate the proposed AVMPPT algorithm. The results show the achievement of the MPP regardless of the region where the maximum peak is located at the P–V curve, the number of peaks, the shape of the shadows, the shadow intensity, the shadow irradiance and the shaded area. An experimental platform to run the tests has been created, Fig. 8. It contains a webcam, three PV modules, a built buck–boost converter with a voltage sensor and a current sensor, a load and a PC, where the artificial vision algorithm is implemented.

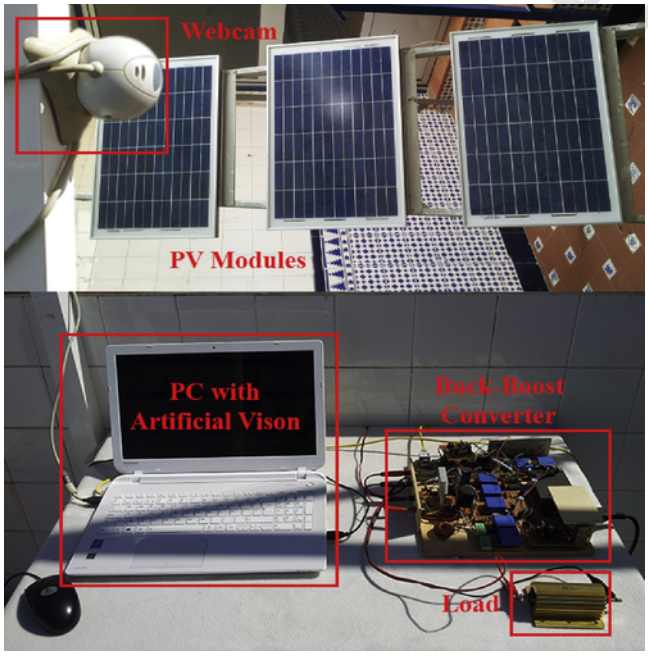

Fig. 8. Experimental platform to validate the artificial vision algorithm.

The Logitech webcam C250 works at a resolution of 800 × 600 pixels and it guarantees a frame rate video capture of up to 30 frames per second (fps). Unlike [20], the camera used in this work is a low-cost webcam because it is about 200 times cheaper than the thermography camera. Besides, if the power plant has a supervision camera, it may be used to detect the shadows, i. e. there is no need to acquire another webcam. The AVMPPT is running in a 2 GHz PC with 2 GB of RAM and the operating system installed is Windows 7. The electrical features of the three solar modules used in the tests were presented in Table 1. The PV modules supply power to a 150 Ω DC load through a DC/DC converter, in this case a built buck–boost converter [26]. Its input voltage value ranges from 10 V to 70 V and the maximum output voltage is 100 V, being 70 W the maximum power that can be transferred. The buck–boost converter diode is the MBR10200 and the MOSFET is the CSD19536KCS driven by a FOD3180 driver. The buck–boost converter efficiency is 92% [24]. Then, LEM sensors measure the voltage and current required by the control. One advantage of this method is that only one current sensor and one voltage sensor at the PV array output are required. The voltage and current measurements at the output of each PV module connected to a bypass diode are not needed.

Then, the backstepping control is implemented in a low-cost microcontroller, the dsPIC30F4011, and it is supervised via a local internet connection through an EM203 serial-to-Ethernet module. The controller manages the MOSFET switching of the buck–boost converter to regulate the PV array output voltage. The control loop sampling time is 10 ms and the PWM frequency is 25 kHz. The platform has a SCADA system to save the data in a .txt file. Then, the data can be used in Matlab to depict the figures.

Several partial shading conditions are tested in the experiments to verify the MPP is achieved under partial shading conditions. The experiments were conducted changing the incident shadow on the PV modules. These changes on the irradiance were not step signals because the clouds usually appear progressively. Fig. 9(a) presents the shadow intensity of three PV modules affected by different irradiances. It shows the shadow intensities directly obtained by the webcam fulfilling Eq. (3). When the shadows change progressively, the shadow intensities change progressively as well. There is a PV module with a shadow intensity of zero, I_{sPV3}, i. e. this solar module is not affected by a shadow, whereas the other two PV modules are partially shaded. One of the partially shaded module has a shadow intensity of approximately 40% from the beginning of the experiment until 67 s, when the shadow disappears. The other partially shaded module reaches a shadow intensity of 60% in an intermittent way because a shadow is appearing and disappearing during the time that the experiment lasts.

Fig. 9(b) shows the shadow irradiance for the different PV modules according to Eq. (4). The solar module with $I_{sPV3} = 0$ is related to a shadow irradiance of 1000 W/m^2. Then, the constant shadow with a shadow intensity of 40% corresponds to $G_{sPV1} = 280$ W/m^2 and the intermittent shadow intensity of 60% is related to 150 W/m^2. In these conditions, three different P–V curves are obtained. From 0 s to 8 s, from 17 s to 28 s and from 40 s to 58 s, a three-peak P–V curve is obtained because two PV modules are partially shaded and one solar module is unshaded. In this case, the maximum power point is located at the first area of the P–V curve, similar to Fig. 3(a). During the intervals ranged from 8 s to 17s, from 28 s to 40 s and from 58 s to 67 s, there is a two-peak P–V curve because only one solar module is partially shaded and the other two modules are unshaded. Now, the MPP is located at the second area of the P–V curve, being the P–V curve similar to Fig. 3(d). Finally, from 67 s to 80 s, the P–V curve has one peak because the partial shading conditions disappeared. Then, the maximum power point is at the third area of the P–V curve. The results of Fig. 9(a) and (b) are summarized in Table 2, detailing the shadow

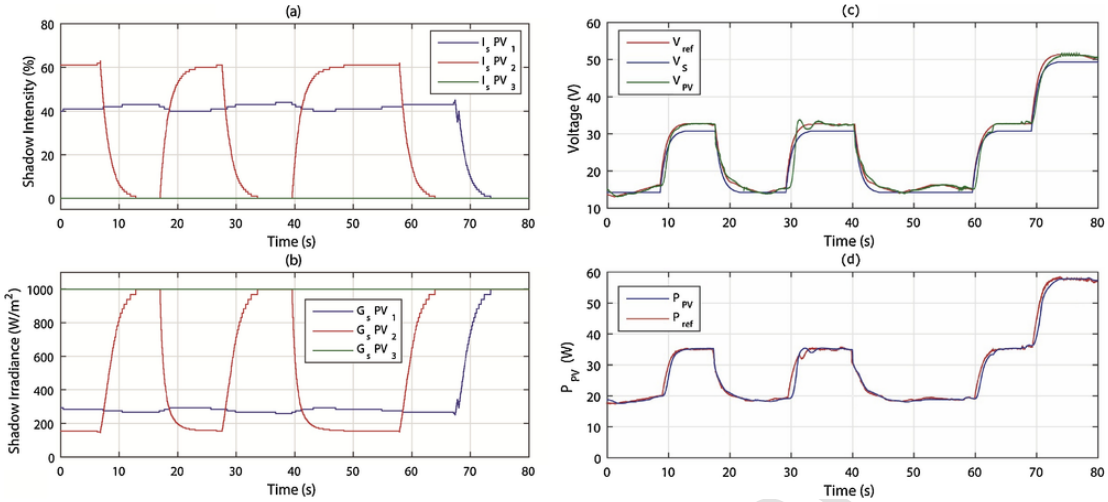

Fig. 9. Experimental results.(a) Shadow intensity for the different PV modules.(b) Shadow irradiance for the three solar modules.(c) Shadow voltage, reference voltage and buck–boost converter input voltage.(d) DC/DC converter input power and the reference power.

Table 2
Shadow intensity and shadow irradiance.

Interval (s)	I_{sPV1} (%)	I_{sPV2} (%)	I_{sPV3} (%)	G_{sPV1} (W/m^2)	G_{sPV2} (W/m^2)	G_{sPV3} (W/m^2)
[0–8)	40	60	0	280	150	1000
[8–17)	40	0	0	280	1000	1000
[17–28)	40	60	0	280	150	1000
[28–40)	40	0	0	280	1000	1000
[40–58)	40	60	0	280	150	1000
[58–67)	40	0	0	280	1000	1000
[67–80]	0	0	0	1000	1000	1000

intensity and the shadow irradiance of each module for each interval of time.

Fig. 9(c) presents the theoretical voltage, v_s, that provides the maximum power by means of the regression plane; the reference voltage achieved by the artificial vision algorithm that should be tracked by the backstepping control, v_{ref}; and the PV modules output voltage, v_{PV}, i.e. the measured voltage at the buck–boost converter input. Thus, three different values of voltage are obtained. When the three-peak P–V curve appears (there are two partially shaded solar modules and one unshaded PV module), the voltage achieved is 14.3 V. When there are two peaks in the P–V curve (one PV module partially shaded and two unshaded solar modules), the voltage obtained is 32 V. Finally, when there is no partial shading, the voltage reached is 51.2 V. It shows how the PV modules output voltage tracks the reference voltage in a fast way, proving the correct performance of the PV system control.

These voltages provide the maximum power, as Fig. 9(d) shows, where the power supplied by the PV system is shown, achieving in all the cases the MPP. The maximum power reached is 18.5 W when v_{PV} is 14.3 V and it is related to the three-peak P–V curve. In the case of the two-peak P–V curve, the power obtained is 35.6 W when the voltage that supplies the maximum power is 32 V. Finally, when the three PV modules are unshaded and there is only one peak in the P–V curve, the maximum power is 58 W for a voltage of 51.2 V. The AVMPPT efficiency (calculated dividing the buck–boost converter input measured power, P_{PV}, by the buck–boost converter input theoretical power, P_{MPP}) is between 98.1% and 99.5%. Fig. 9(c) and (d) are summarized in Table 3.

Fig. 10 depicts the control signal of the backstepping controller. It shows that signal is smooth. Besides, when there is a change in the shadows, the response of the controller does not have oscillations.

Table 3
Experimental test results.

Interval (s)	No. of peaks	V_{PV} (V)	P_{MPP}	P_{PV} (W)
[0–8)	3	14.3	18.6	18.5
[8–17)	2	32	36	35.6
[17–28)	3	14.3	18.6	18.5
[28–40)	2	32	36	35.6
[40–58)	3	14.3	18.6	18.5
[58–67)	2	32	36	35.6
[67–80]	1	51.2	59.1	58

Fig. 11 shows how the artificial vision algorithm detects the partial shading conditions, similar to Fig. 6. Two different cases of the experimental test are presented. Fig. 11(a) corresponds to the previous three-peak P–V curve, where two PV modules are partially shaded with different shadow irradiances, 280 W/m^2 and 150 W/m^2, and the third module is unshaded with an irradiance of 1000 W/m^2. The webcam detects the area that it is partially shaded in the first two PV modules using HSV thresholding and the blob detection. Table 4 presents the HSV color values for the thresholding used to detect the PV modules shadows. Fig. 11(b) is related to the previous two-peak P–V curve in the intervals ranged from 8 s to 17s, from 28 s to 40 s and from 58 s to 67 s because only one solar module is affected by a shadow as it is detected by the artificial vision algorithm. The shadow irradiance of the partially shaded PV module is 280 W/m^2 and the incident irradiance in the other two unshaded modules is 1000 W/m^2.

Another set of experiments have been carried out. In this case, all the PV modules are affected by the shadows in different instants of time. Figs. 12(a) and (b) show the shadow intensity and the shadow irradiance, respectively, achieved for the three PV modules. Table 5 presents the results related to I_{sPVj} and G_{sPVj}. The experiment is divided

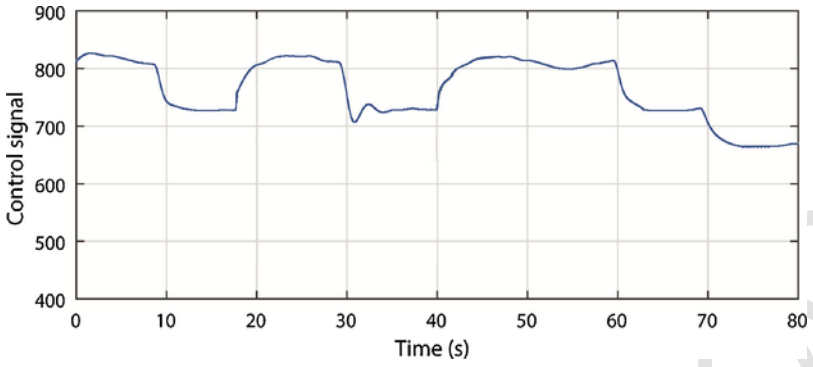

Fig. 10. Control signal.

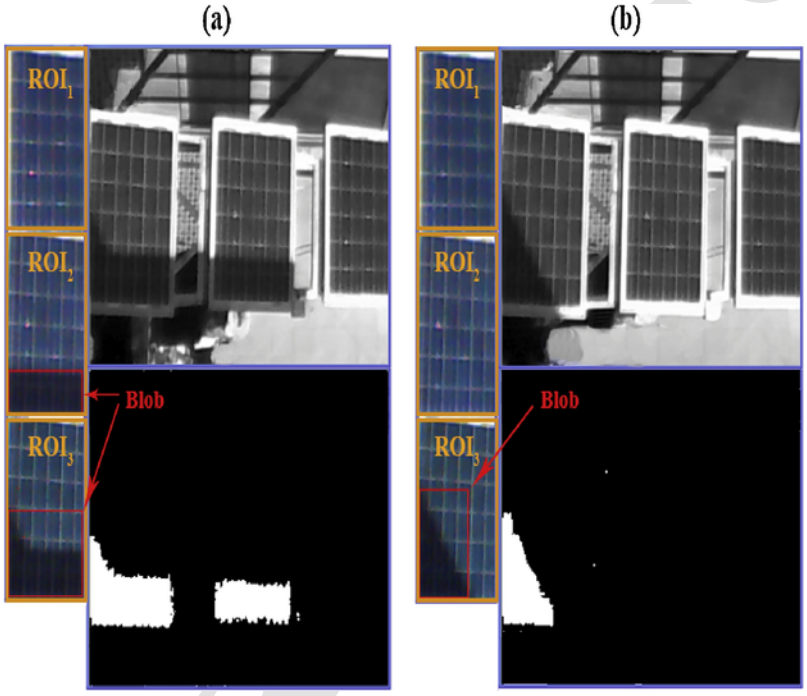

Fig. 11. Detection of the shadows.(a) Shadow detection when two PV modules are shaded.(b) Shadow detection of one shaded solar module.

Table 4
HSV threshold values.

Parameter	Min	Max
Hue (H)	81	256
Saturation (S)	60	256
Value (V)	0	96

into four main intervals obtaining different values of power. In the first three intervals, there are three-peak P–V curves, and the last interval is related to a one-peak P–V curve because the PV modules are not affected by shadows. Among these intervals, there are some changes in the shadows that cause variations in the shadow intensity and the shadow irradiance values, as shows Fig. 12(a) and (b).

Fig. 12(c) depicts the theoretical voltage, v_s; the reference voltage achieved by the artificial vision algorithm, v_{ref}; and the PV modules output voltage, v_{PV}. As it was explained for Fig. 11 (c), the voltages obtained depends on the area of the P–V curve where the MPP is located. From 0 s to 19 s, there are three shaded modules and the maximum peak is located at the third area of the P–V curve, obtaining a value of 45.5 V, similar to Fig. 3(c). Then, from 19 s to 48 s and from 48 s to 86 s, there is one unshaded PV module and the other two modules are shaded. The MPP is located at the first area of the P–V curve with a voltage of 18.1 V and 19.5 V respectively, similar to Fig. 3(a). Finally, from 86 s on, the shadows start to disappear and there is only one peak in the P–V curve with a voltage of 50 V. Among the main intervals, there are transition times when the shaded PV modules become unshaded or vice versa. This figure presents the appropriate performance of the control because the PV modules output voltage tracks the reference voltage in a fast way. Fig. 12(d) presents the maximum power obtained for the different conditions and the reference power. When the three PV modules are shaded, the MPP reaches its minimum value, 4.1 W. If there is a PV module unshaded, the MPP is 12.3 W and 14.7 W whereas if all the PV modules are unshaded, the maximum power is higher, 49.9 W. Fig. 12(d) shows how the measured power is similar to the reference power, proving the accuracy of the control algorithm. The efficiency in this experiment ranges from 98.3% to 99.6%. These results are presented in Table 6.

The control signal for this set of experiments is presented in Fig. 13. The signal is smooth and under perturbations the signal does not have oscillations.

The shadows are continuously changing and the obtained results show that they are adjusted properly in real time. Thus, this require-

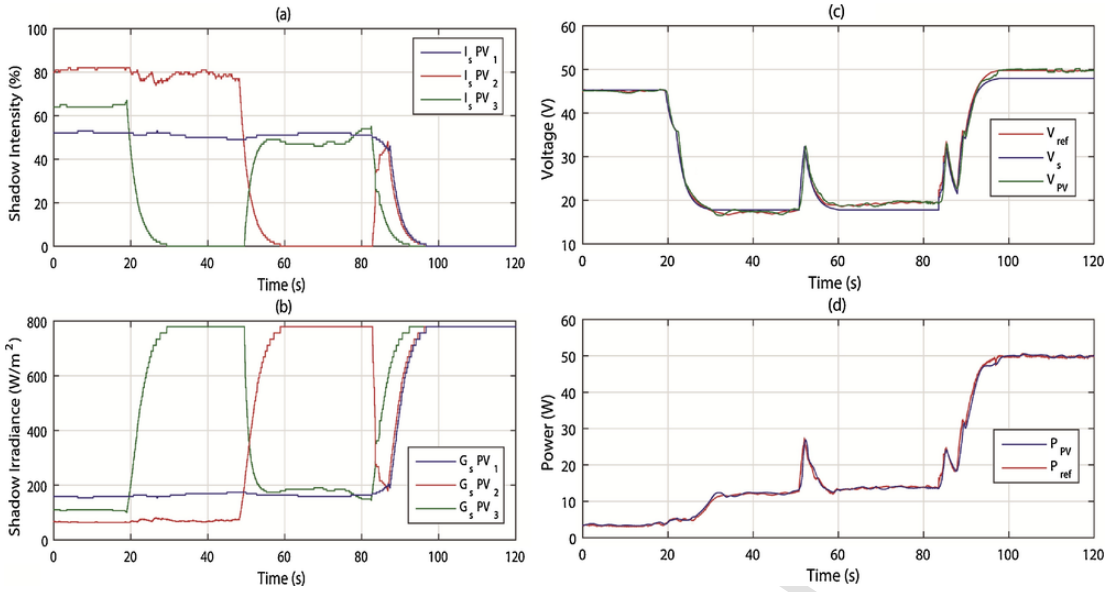

Fig. 12. Experimental results.(a) Shadow intensity for the different PV modules.(b) Shadow irradiance for the three solar modules.(c) Shadow voltage, reference voltage and buck–boost converter input voltage.(d) DC/DC converter input power and the reference power.

Table 5
Shadow intensity and shadow irradiance.

Interval (s)	I_{sPV1} (%)	I_{sPV2} (%)	I_{sPV3} (%)	G_{sPV1} (W/m^2)	G_{sPV2} (W/m^2)	G_{sPV3} (W/m^2)
[0–19)	52	80	63	160	80	105
[19–48)	52	80	0	160	80	780
[48–86)	52	0	47	160	780	196
[86–120]	0	0	0	780	780	780

Table 6
Experimental test results.

Interval (s)	No. of peaks	V_{PV} (V)	P_{MPP}	P_{PV} (W)
[0–19)	3	45.5	4.17	4.1
[19–48)	3	18.1	12.5	12.3
[48–83)	3	19.5	14.9	14.7
[83–120]	1	50	50.1	49.9

ment is fulfilled. Besides, the expected results are obtained (such as the simulated results predicted in the simulations) and they are achieved with a high efficiency. The MPPT performance is between 98.1% and 99.6%, whereas other methods, such as the Thermography-Based Virtual MPPT, [20], has a MPPT error between 3.9% and 4.4%; or the DEPSO method, [16], has a tracking efficiency between 97.5% and 98.2%.

5. Conclusion

This work proposes a novel artificial vision algorithm to detect partial shading conditions affecting solar modules in a PV system. It also provides the reference voltage to a non-linear backstepping control. This control regulates the PV modules output voltage controlling the duty cycle of a buck–boost converter to reach the maximum power point. Thus, the algorithm is able to avoid local maxima and it leads the voltage directly to the area of the P–V curve where the global maximum is located.

Two new parameters are defined, the shadow intensity and the shadow irradiance. The shadow intensity is the mean value of the grey level of the shaded area whereas the shadow irradiance is the irradiance level of the shadow. Thus, the artificial vision algorithm provides

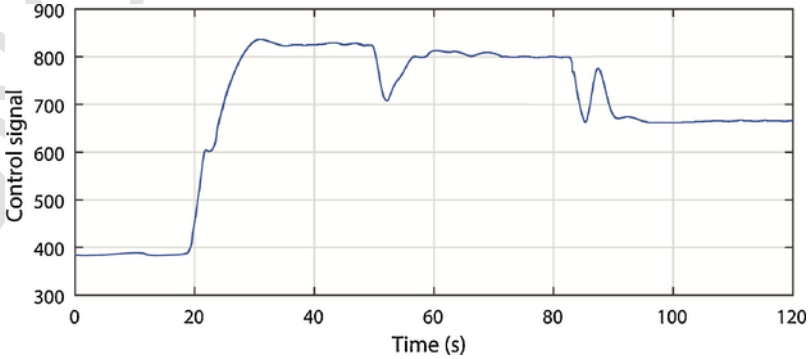

Fig. 13. Control signal.

the shadow irradiance of each solar module, the area affected by partial shading and the voltage that supplies the maximum power.

The first advantage of this method is the use of a low-cost camera to detect the shadows or even it can use the camera for surveillance in the PV power plants. Moreover, this method only needs one voltage sensor and one current sensor at the PV array output and it is not required the use of several sensors to measure the voltage and current at the output of each PV module across a bypass diode.

Experimental results present the performance of the PV system using artificial vision algorithm with the backstepping control. The tracking efficiency is between 98.1% and 99.6%. Results validate the detection of the shadows, the calculation of the shadow irradiance and the achievement of the maximum power point under partial shading conditions. The global maximum is always reached regardless of where it is located and the number of peaks of the P–V curve.

As future work, a low-cost embedded system will be studied to include the operating system with the webcam drivers and the libraries for the vision algorithm as well as the implementation of the backstepping controller. A Raspberry Pi could be used because it has a high computation capacity and it is able to execute the whole algorithm.

References

[1] Y. Tian, B. Xia, Z. Xu, et al., Modified asymmetrical variable step size incremental conductance maximum power point tracking method for photovoltaic systems, J. Power Electron. 14 (1) (2014) 156–164.

[2] T. Esram, P.L. Chapman, Comparison of photovoltaic array maximum power point tracking techniques, IEEE Trans. Energy Convers. 22 (2) (2007) 439–449.

[3] M.L. Orozco-Gutierrez, G. Petrone, J.M. Ramirez-Scarpetta, G. Spagnuolo, C.A. Ramos-Paja, A method for the fast estimation of the maximum power points in mismatched PV strings', Electr. Power Syst. Res. 121 (2015) 115–125.

[4] S. Moballegh, J. Jiang, Modeling, prediction, and experimental validations of power peaks of PV arrays under partial shading conditions, IEEE Trans. Sustain. Energy 5 (1) (2014) 293–300.

[5] G. Petrone, C.A. Ramos-Paja, 'Modeling of photovoltaic fields in mismatched conditions for energy yield evaluations', Electr. Power Syst. Res. 81 (2011) 1003–1013.

[6] M.Z.S. El-Dein, M. Kazerani, M.M.A. Salama, Optimal photovoltaic array reconfiguration to reduce partial shading losses, IEEE Trans. Sustain. Energy 4 (1) (2013) 145–153.

[7] I.R. Balasubramanian, S.I. Ganesan, N. Chilakapati, Impact of partial shading on the output power of PV systems under partial shading conditions, IET Power Electron. 7 (3) (2014) 657–666.

[8] R.P. Vengatesh, S.E. Rajan, Investigation of the effects of homogeneous and heterogeneous solar irradiations on multicrystal PV module under various configurations, IET Renew. Power Gener. 9 (3) (2015) 245–254.

[9] H. Zhenga, S. Lia, R. Challoob, et al., Shading and bypass diode impacts to energy extraction of PV arrays under different converter configurations, Renew. Energy 68 (2014) 58–66.

[10] H. Patel, V. Agarwal, MATLAB-based modeling to study the effects of partial shading on PV array characteristics, IEEE Trans. Energy Convers. 23 (1) (2008) 302–310.

[11] Y. Yi, J. Sheng-lan, G. Hai-qin, et al., Simulation study on characteristics of photovoltaic array under partial shading, In: Presented at. 33rd Chinese Control Conf., Nanjing, China, 2014, pp. 6992–6997.

[12] K. Sundareswaran, V. Vigneshkumar, S. Palani, Development of a hybrid genetic algorithm/perturb and observe algorithm for maximum power point tracking in photovoltaic systems under non-uniform insolation, IET Renew. Power Gener. 9 (7) (2015) 757–765.

[13] N.E. Zakzouk, M.A. Elsaharty, A.K. Abdelsalam, A.A. Helal, B.W. Williams, Improved performance low-cost incremental conductance PV MPPT technique, IET Renew. Power Gener. 10 (4) (2016) 561–574.

[14] Syafaruddin, E. Karatepe, T. Hiyama, Artificial neural network-polar coordinated fuzzy controller based maximum power point tracking control under partially shaded conditions, IET Renew. Power Gener. 3 (2) (2009) 239–253.

[15] R. Arulmurugana, N. Suthanthiravanitha, Model and design of a fuzzy-based Hopfield NN tracking controller for standalone PV applications, Electr. Power Syst. Res. 120 (2015) 184–193.

[16] M. Seyedmahmoudian, R. Rahmani, S. Mekhilef, et al., Simulation and hardware implementation of new maximum power point tracking technique for partially shaded PV system using hybrid DEPSO method, IEEE Trans. Sustain. Energy 6 (3) (2015) 850–862.

[17] Y.J. Wang, S.S. Lin, Analysis of a partially shaded PV array considering different module connection schemes and effects of bypass diodes, In: Presented at ICUE, Pattaya City, Thailand, 2011, pp. 1–7.

[18] M.E. Nezhad, B. Asaei, S. Farhangi, Modified analytical solution for tracking photovoltaic module maximum power point under partial shading condition, In: Presented at 13th EEEIC, Wroclaw, Poland, 2013, pp. 182–187.

[19] A. Nabil, M. Miyatake, A novel maximum power point tracking for photovoltaic applications under partially shaded insolation conditions, Electr. Power Syst. Res. 78 (2008) 777–784.

[20] Y. Hu, W. Cao, J. Wu, et al., Thermography-based virtual MPPT scheme for improving PV energy efficiency under partial shading conditions, IEEE Trans. Power Electron. 29 (11) (2014) 5667–5672.

[21] S.L. Ching, M. Sabudin, Website image colour transformation for the colour blind, In: Presented at 2nd ICCTD, Cairo, Egypt, 2010, pp. 255–259.

[22] F.Y. Shih, H. Wu, Decomposition of geometric-shaped structuring elements using morphological transformations on binary images, In: Presented at 11th Annual Int. Phoenix Conf. on Computers and Communications, Scottsdale, United States, 1992, pp. 356–363.

[23] T.B. Nguyen, S.T. Chung, An improved real-time blob detection for visual surveillance, In: Presented at 2nd Int. CISP, Tianjin, China, 2009, pp. 1–5.

[24] A.D. Martin, J.M. Cano, J.F.A. Silva, J.R. Vazquez, 'Backstepping control of smart grid-connected distributed photovoltaic power supplies for telecom equipment', IEEE Trans. Energy Convers. 30 (4) (2015) 1496–1504.

[25] A.D. Martin, J.R. Vazquez, Backstepping controller design to track maximum power in photovoltaic systems, Automatika 55 (1) (2014) 22–31.

[26] J.R. Vazquez, A.D. Martin, Backstepping control of a buck–boost converter in an experimental PV-system, J. Power Electron. 15 (6) (2015) 1584–1592.

[27] M. Valipour, Optimization of neural networks for precipitation analysis in a humid region to detect drought and wet year alarms, Meteorol. Appl. 23 (1) (2016) 91–100, 2016.

[28] M. Valipour, M.E. Banihabib, S.M.R. Behbahani, Comparison of the ARMA, ARIMA, and the autoregressive artificial neural network models in forecasting the monthly inflow of Dez dam reservoir, J. Hydrol. 476 (7) (2013) 433–441.

[29] M. Valipour, M.A.G. Sefidkouhi, S. Eslamian, Surface irrigation simulation models: a review, Int. J. Hydrol. Sci. Technol. 5 (1) (2015).

[30] M. Valipour, Sprinkle and trickle irrigation system design using tapered pipes for pressure loss adjusting, J. Agric. Sci. 4 (12) (2012).

[31] M.M. Khasraghi, M.A.G. Sefidkouhi, M. Valipour, Simulation of open- and closed-end border irrigation systems using SIRMOD, Arch. Agron. Soil Sci. 61 (7) (2015) 929–941.